MOLECULAR IMAGING AND BIOLOGY

Mol Imaging Biol (2014) 16:793–801
DOI: 10.1007/s11307-014-0752-1

Published Online: 2 July 2014

World Molecular Imaging Society

RESEARCH ARTICLE

Dimeric [^{68}Ga]DOTA-RGD Peptide Targeting $\alpha_v\beta_3$ Integrin Reveals Extracellular Matrix Alterations after Myocardial Infarction

Max Kiugel,[1] Ingrid Dijkgraaf,[2] Ville Kytö,[3] Semi Helin,[1,4] Heidi Liljenbäck,[1,5] Tiina Saanijoki,[1] Cheng-Bin Yim,[1,4] Vesa Oikonen,[1] Pekka Saukko,[6] Juhani Knuuti,[1] Anne Roivainen,[1,5] Antti Saraste[1,3,7]

[1]*Turku PET Centre, Turku University Hospital, University of Turku, Kiinamyllynkatu 4-8, 20520, Turku, Finland*
[2]*Department of Biochemistry, University of Maastricht, Maastricht, The Netherlands*
[3]*Heart Center, Turku University Hospital, University of Turku, Turku, Finland*
[4]*Åbo Akademi University, Turku, Finland*
[5]*Turku Center for Disease Modeling, University of Turku, Turku, Finland*
[6]*Department of Forensic Medicine, University of Turku, Turku, Finland*
[7]*Institute of Clinical Medicine, University of Turku, Turku, Finland*

Abstract

Purpose: We evaluated a dimeric RGD-peptide, [^{68}Ga]DOTA-E-[c(RGDfK)]$_2$, for positron emission tomography (PET) imaging of myocardial integrin expression associated with extracellular matrix remodeling after myocardial infarction (MI) in rat.

Procedures: Male Sprague-Dawley rats were studied at 7 days and 4 weeks after MI induced by permanent ligation of the left coronary artery and compared with sham-operated controls.

Results: In vivo imaging revealed higher tracer uptake in the infarcted area than in the remote non-infarcted myocardium of the same rats both at 7 days (MI/remote ratio, 2.25±0.24) and 4 weeks (MI/remote ratio, 2.13±0.37) post-MI. Compared with sham-operated rats, tracer uptake was higher also in the remote, non-infarcted myocardium of MI rats both at 7 days and 4 weeks where it coincided with an increased interstitial fibrosis. Standardized uptake values correlated well with the results of tracer kinetic modeling. Autoradiography confirmed the imaging results showing 5.1 times higher tracer uptake in the infarcted than remote area. Tracer uptake correlated with the amount of β_3 integrin subunits in the infarcted area.

Conclusions: Our results show that integrin-targeting [^{68}Ga]DOTA-E-[c(RGDfK)]$_2$ is a potential tracer for monitoring of myocardial extracellular matrix remodeling after MI using PET.

Key words: Integrin, Myocardial infarction, PET, Rat, RGD

Introduction

Integrins are cell membrane glycoprotein receptors that are among other things expressed in the myocardium during extracellular matrix (ECM) remodeling after myocardial infarction (MI). Their expression has been associated with

Electronic supplementary material The online version of this article (doi:10.1007/s11307-014-0752-1) contains supplementary material, which is available to authorized users.

Correspondence to: Antti Saraste; *e-mail:* antti.saraste@utu.fi

inflammation, angiogenesis [1, 2], and fibrosis [3, 4]. Targeted radiolabeled peptides containing the arginine-glycine-aspartic acid (RGD) can detect the upregulation of integrins after ischemic myocardial injury [1, 2, 4, 5]. After an ischemic injury, $\alpha_v\beta_3$ integrin is expressed by endothelial cells and myofibroblasts in the damaged myocardium and may reflect post-infarct healing processes [1–3]. Increased uptake of RGD peptides extending to the remote non-infarcted areas, outside the scar area has been shown in some [4], but not in all studies [1, 2, 5]. Molecular imaging of $\alpha_v\beta_3$ integrin may be useful for imaging ECM remodeling during MI healing process and left ventricle (LV) remodeling.

Multimerization of RGD domains increases the affinity and uptake of tracers [6]. The binding affinity of recently developed ^{68}Ga-labeled dimeric RGD tracer, [^{68}Ga]DOTA-E-[c(RGDfK)]$_2$, as determined in a solid-phase competitive binding assay, was about fivefold higher compared to [^{68}Ga]DOTA-RGD monomer [7]. The dimeric RGD peptide exhibited improved tumor targeting compared to the monomeric RGD peptide [7]. Competitive binding assays indicated that the tracer is specific for $\alpha_v\beta_3$ integrin [8]. Compared to other positron-emitting radionuclides, advantages of ^{68}Ga are in its cheaper production (elution from ^{68}Ga/^{68}Ge generator) and redundancy of an on-site cyclotron. However, lower positron yield (89 %) and higher β+energy (Emax= 1,899 keV) compared with ^{18}F (97 % and 633 keV) results in lower spatial resolution of positron emission tomography (PET) images. Radiolabeled integrin targeting peptides used for cardiac imaging include [^{111}In]-RP748 [1], [^{99m}Tc]-NC100692 [9], [^{99m}Tc]-CRIP [4], [^{18}F]-galacto-RGD [2, 5], [^{18}F]-A1F-NOTA-PRGD2 [10], as well as ^{68}Ga-labeled RGD conjugates [11, 12]. Dimeric RGD tracers as well as ^{68}Ga-labeled tracers are still relatively new to the field and their feasibility for imaging cardiac $\alpha_v\beta_3$ integrin need to be tested.

We evaluated [^{68}Ga]DOTA-E-[c(RGDfK)]$_2$ for in vivo imaging of myocardial ECM remodeling after MI. Infarction was induced in rats by surgical ligation of the left coronary artery (LCA) and [^{68}Ga]DOTA-E-[c(RGDfK)]$_2$ uptake was studied in both early (7 days) and late (4 weeks) phases after MI. The in vivo uptake was measured by a dedicated small-animal PET and compared with anatomical information obtained with computed tomography (CT) as well as the results of myocardial perfusion imaging with [^{11}C]-acetate. To confirm [^{68}Ga]DOTA-E-[c(RGDfK)]$_2$ uptake, autoradiography of LV tissue sections was performed and compared with collagen deposition, neovascularization, macrophages, and the presence of β_3 integrin subunits in these sections.

Material and Methods

Animal Model and Study Design

The study protocol was approved by the Lab-Animal Care and Use Committee of the State Provincial Office of Southern Finland. In total, 38 male Sprague-Dawley rats (age, 8±1 weeks; weight, 320±65 g) were used.

MI was induced in anesthetized rats by surgical ligation of the LCA via thoracotomy [13, 14]. Refer to the Online Supplementary Material for further details. The sham operation consisted of all the same protocols except the closure of LCA. Operative mortality in both coronary ligation and sham groups was approximately 25 % and occurred during the first 2 days.

The rats were studied at 7 days (n=8) or 4 weeks (n=7) after coronary ligation or at 7 days (n=5) or 4 weeks (n=3) after the sham operation. The rats were injected with 46±7.8 MBq (1.9±0.8 nmol, 150−500 μl) of [^{68}Ga]DOTA-E-[c(RGDfK)]$_2$ via tail vein. Seventy-five minutes post-injection, ex vivo biodistribution of [^{68}Ga]DOTA-E-[c(RGDfK)]$_2$ was analyzed in tissue samples and myocardial uptake was studied by autoradiography of LV tissue sections.

A subset of these rats [7 days (n=5) or 4 weeks (n=5) post-MI and 7 days (n=3) or 4 weeks (n=2) after sham operation] underwent 60-min dynamic [^{68}Ga]DOTA-E-[c(RGDfK)]$_2$ PET and contrast-enhanced CT in order to evaluate kinetics of myocardial tracer uptake. On the same day, two rats in each group were PET imaged with [^{11}C]-acetate to evaluate myocardial perfusion and to localize infarcted area (Supplementary Material).

Radiochemistry

DOTA-E-[c(RGDfK)]$_2$ precursor was synthesized and radiolabeled with ^{68}Ga as described before [7, 15, 16]. Refer to the Supplementary Material for molecular structure (Fig. S1) and details of synthesis. In vivo stability of [^{68}Ga]DOTA-E-[c(RGDfK)]$_2$ was studied in rat blood and urine by radio-HPLC (refer to the Supplementary Material). [^{11}C]-acetate was synthesized as described previously [17].

Ex Vivo Biodistribution

Immediately after PET/CT, at 75 min after tracer injection, animals were killed by cervical dislocation, blood samples were obtained by cardiac puncture and various tissues were excised, weighed, and measured for radioactivity using a gamma counter (Triathler 3″, Hidex, Turku, Finland). Radioactivity values were normalized by injected radioactivity dose, decay with a delta time between injection and measurement, animal weight, and the weight of tissue sample. Results were expressed as standardized uptake values (SUV).

Autoradiography

The LV was frozen in cooled isopentane and sliced into serial transverse cryosections of 8-μm (for immunohistochemistry) and 20-μm at 1-mm intervals (five to six intervals per heart) from apex to base. Uptake of [^{68}Ga]DOTA-E-[c(RGDfK)]$_2$ in the infarcted and remote myocardium were analyzed by autoradiography of tissue sections as described previously [18–20]. For more details, see the Supplementary Material.

Histology and Immunohistochemistry

After autoradiography, the serial LV cryosections were stained with hematoxylin-eosin (HE) for general histology and evaluation of MI size as described earlier [5]. Masson's trichrome staining was used to distinguish collagen from myocytes. Macrophages, endothelial cells, and β_3 integrin subunits were detected by immunohistochemical staining using the CD68, CD31, and CD61 antibodies, respectively. For details, see Supplementary Material. Uptake of [^{68}Ga]DOTA-E-[c(RGDfK)]$_2$ was compared with the area percentage of CD31, CD68, or CD61 staining within the area of MI scar measured by Image-Pro Plus v.7.0 software (Media Cybernetics Inc., Bethesda, MD, USA). Uptake of [^{68}Ga]DOTA-E-[c(RGDfK)]$_2$ was also compared with the amount of collagen measured as area percentage in tissue sections stained with Masson's trichrome.

PET/CT

The rats were imaged using a small-animal PET/CT (Inveon Multimodality; Siemens Medical Solutions, Knoxville, TN, USA). The rats were anesthetized using 1.5 % isoflurane, the electrocardiogram was monitored, and temperature was maintained using a heating pad throughout the imaging. Immediately after PET, 200 μl of intravascular iodinated contrast agent eXIATM160XL (Binitio Biomedical Inc, Ottawa, ON, Canada) was injected and high-resolution CT was acquired. For details, see Supplementary Material.

Alignment of PET and CT images was automatic and confirmed visually by anatomical landmarks. Image analysis was done using Carimas v.2.5 software (Turku PET Centre, Turku, Finland). Data were normalized and corrected for injected radioactivity dose and radionuclide decay. Several regions of interest (ROIs) were defined according to high-resolution CT image: (1) infarcted zone (verified by corresponding HE stained histological sections or [^{11}C]-acetate perfusion images), (2) remote myocardium in the septum, (3) blood pool (inside LV), (4) chest wall scar, (5) liver, and (6) lungs. Myocardial ROIs in sham-operated rats were defined in the septum for comparison with remote myocardium and in anterior wall for comparison with infarcted area in order to compensate for potential spill-over activity from the chest wall wound. Results were reported as mean radioactivity concentration (Bq/ml) as a function of time after injection, i.e., as time-activity curves (TACs).

Modeling of PET Data

The dynamic [^{68}Ga]DOTA-E-[c(RGDfK)]$_2$ PET data was analyzed by graphical Logan method and compartmental modeling [21, 22]. The blood TAC obtained from heart LV was converted to plasma TAC using mean plasma/blood ratio of radioactivity 1.64±0.16 (range, 1.28−1.88) measured from the blood samples taken immediately after PET imaging. The image-derived input function was further corrected with parent fractions, measured from separate animals, two to three per time point. Logan plots were calculated using either the metabolite-corrected plasma or total plasma as input to compare if metabolite correction is necessary when data is collected only up to 60 min. Two-tissue compartmental models were fitted to data, weighting data by sample frequency only. Fitting limits were changed from the default because it was expected that blood volume may be very high in these tissue types, and some tissues may also include high spillover from heart cavities. Compartmental model results in the remote LV area (=septum) were not taken into account due to spillover from both ventricles. Parametric images of distribution volumes were obtained by using Logan plots. Modeling images and data were compared with SUVs.

Statistical Analysis

All data are expressed as mean±SD. Statistical analysis was done with SPSS Statistics software v. 21 (IBM, NY, USA). An unpaired Student's t test was applied for comparisons between two groups, and paired Student's t test was applied for comparisons within each group. Comparisons of three groups were done using ANOVA with Dunnett's correction for control group. Spearman's rank test (r_s) was used to analyze correlation between two continuous variables. p values less than 0.05 were considered statistically significant.

Results

Characteristics of Animals

None of the sham-operated rats had evidence of MI. In contrast, all rats with coronary occlusion had MI as confirmed with histological analysis. Average MI size measured as the percentage of the LV circumference was 38±23 % (range, 12–67) at 7 days and 51±16 % (range, 12–62) at 4 weeks (p=0.3). Histology (Figs. 1 and 2) demonstrated a necrotic core surrounded by granulated tissue containing abundant myofibroblasts, neovessels, and macrophages at 7 days after coronary ligation. A collagenous scar was present at 4 weeks after ligation. Masson's trichrome staining demonstrated that the scar tissue contained less dense collagen at 7 days than at 4 weeks after MI (52±10 % of area vs. 68±8.2 % of area, p=0.04). As shown in Fig. 2i, there was more interstitial collagen in the remote, non-infarcted myocardium by 4 weeks after MI than in sham-operated rats (3.0±1.2 % vs. 1.7±0.4 % of area (p=0.07) and 4.3±2.7 % vs. 1.7±0.2 % of area (p=0.03)).

Radiochemistry

The radiochemical purity and specific radioactivity of [^{68}Ga]DOTA-E-[c(RGDfK)]$_2$ were ≥95 % and 64±42 MBq/nmol (n=17), respectively. [^{68}Ga]DOTA-E-[c(RGDfK)]$_2$ peptide showed feasible in vivo stability with the proportion of total radioactivity in plasma originating from the intact tracer being 94±3.2 % at 45 min after injection and 68±6.1 % at 60 min (Fig. S2b in the Supplementary Material). Only one radioactive metabolite was detected. Under the described radio-HPLC conditions, the retention time for intact [^{68}Ga]DOTA-E-[c(RGDfK)]$_2$ and the radiometabolite were 11.5 and 3.5 min, respectively. Retention time of 3.5 min most probably indicates the

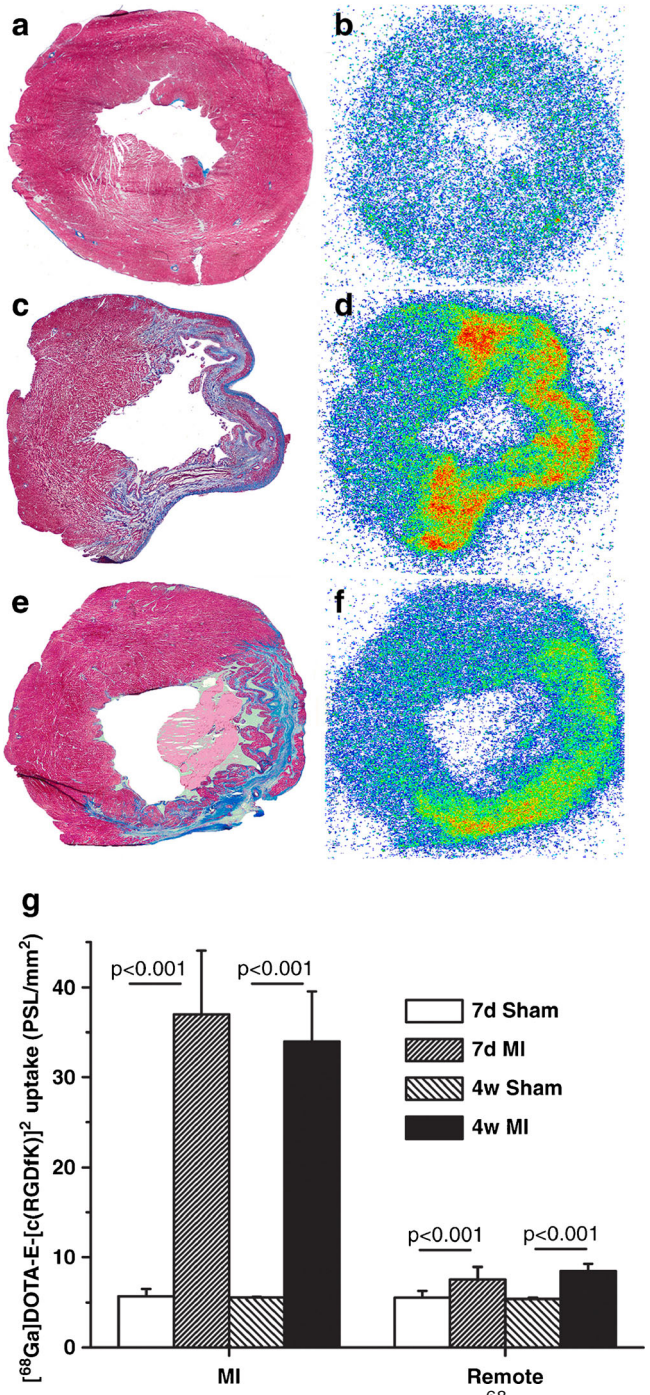

Fig. 1. Autoradiography of myocardial [^{68}Ga]DOTA-E-[c(RGDfK)]$_2$ uptake. Serial tissue sections stained with Masson's trichrome (a, c, e) and autoradiographs (b, d, f) show minimal tracer uptake in the myocardium of sham-operated rat (a, b), but there is regionally increased uptake (green and red) co-localizing with the infarct scar both at 7 days (c, d) and 4 weeks (e, f) after permanent coronary ligation. (g) The results of quantification of tracer uptake. Compared with sham-operated controls, there was increased tracer uptake in the infarcted area (MI) and also in the remote non-infarcted myocardium both at 7 days and 4 weeks post-MI.

metabolite as a detached DOTA chelator. The radioactivity was rapidly excreted through kidneys and appeared >98 % as intact tracer in urine at 75 min after injection.

Ex Vivo Biodistribution

Compared with sham-operated rats, [^{68}Ga]DOTA-E-[c(RGDfK)]$_2$ uptake in the LV myocardium (including both infarct and remote myocardium) was 2.2-fold higher at 7 days post-MI [n=5, p<0.001 (SUV, 0.52±0.13 vs. 0.24±0.01)] and 2.4-fold higher at 4 weeks post-MI [n=6, p<0.001 (SUV, 0.53±0.09 vs. 0.23±0.03)]. Average myocardium/blood ratio was 3.6±1.7 (p=0.01) at 7 days post-MI and 2.9±1.8 at 4 weeks (p<0.001). Detailed biodistribution results are shown in Fig. S2a in the Supplementary Material.

Autoradiography

A representative autoradiograph of myocardial [^{68}Ga]DOTA-E-[c(RGDfK)]$_2$ uptake is shown in Fig. 1. In the myocardium of sham-operated rats, uptake was low throughout the myocardium both at 7 days and at 4 weeks after operation. There was focally increased [^{68}Ga]DOTA-E-[c(RGDfK)]$_2$ uptake in the anterolateral wall of the LV co-localizing with the infarct scar in all rats with coronary ligation. Quantitatively, the average [^{68}Ga]DOTA-E-[c(RGDfK)]$_2$ uptake in the infarcted area was 6.5-fold higher than in the corresponding myocardium of sham-operated rats (37±7.0 vs. 5.7±0.8 PSL/mm^2, p<0.001) and 5.1±1.6 (p<0.001)-fold higher than in the remote non-infarcted myocardium of rats with coronary ligation at 7 days post-MI. At 4 weeks post-MI, the uptake was still 6.1-fold higher (34±0.6 vs. 5.5±0.1 PSL/mm^2, p<0.001: Fig. 1g) than in sham-operated rats and 4.1±1.0 (p<0.001)-fold higher than in the remote myocardium. Tracer uptake was also increased in the remote, non-infarcted myocardium both at 7 days and 4 weeks post-MI as compared with the corresponding myocardial wall of sham-operated rats (7.5±1.4 vs. 5.5±0.7 PSL/mm^2, p=0.006 and 8.5±0.8 vs. 5.4±0.1 PSL/mm^2, p<0.001, respectively).

In Vivo PET/CT

In vivo [^{68}Ga]DOTA-E-[c(RGDfK)]$_2$ PET/CT images showed focally increased tracer uptake in the LV myocardium at 7 days and 4 weeks post-MI co-localizing with the perfusion defect area in the [^{11}C]acetate images (Fig. 3). TAC analysis revealed the kinetics of tracer accumulation and elimination with optimal myocardium/blood ratio starting at 45 min post-injection (Fig. 3m–o). Table 1 shows myocardial and blood uptakes of tracer as average SUV values measured at 45–60 min post-injection in vivo. There was increased tracer uptake in the infarcted area at 7 days (MI/remote ratio 2.25±0.24, p<0.001) and 4 weeks (MI/

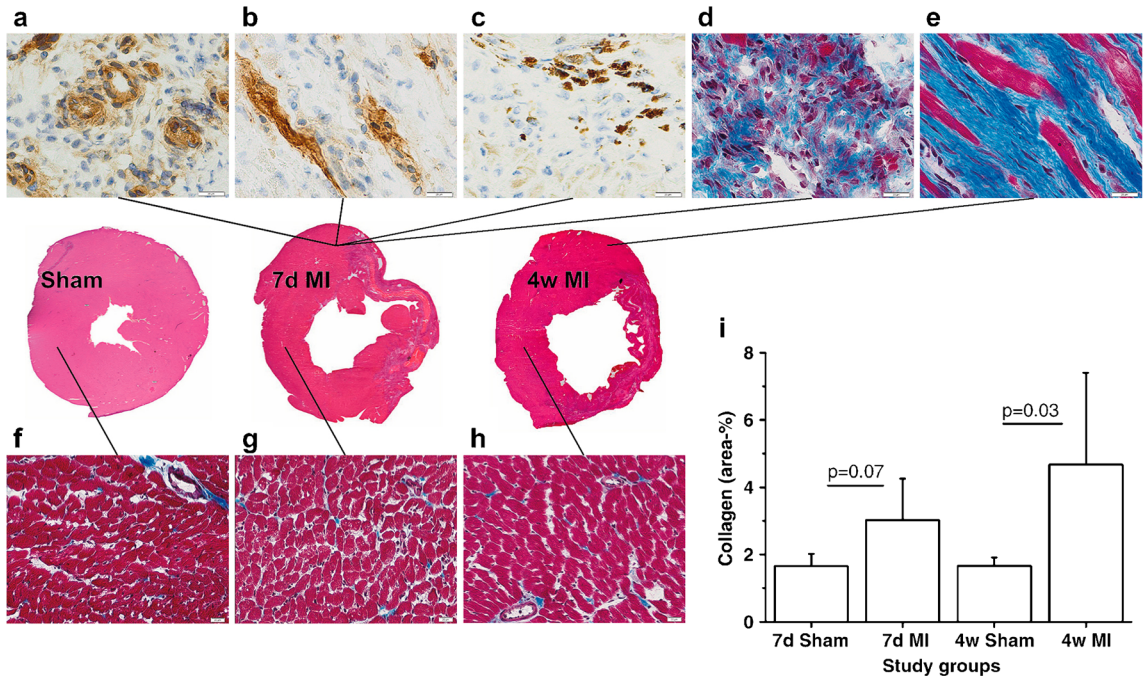

Fig. 2. Myocardial histology and immunohistochemistry after infarction in rats. High magnification photomicrographs show brown staining of CD31-positive endothelial cells lining the capillaries (a), β_3 integrin (CD61) (b), and macrophages (CD68) (c) in the infarcted area. Masson's trichrome staining of collagen fibers shows replacement fibrosis in the infarct area at 7 days (d) and 4 weeks after MI (e). Note the dense collagenous scar at 4 weeks. In the remote non-infarcted myocardium, diffuse interstitial fibrosis is present 7 days and 4 weeks after MI (f–h). Graph shows that the area percentage of collagen fibers in the remote myocardium was higher 4 weeks after MI as compared with sham-operated rats. Scale bars 20 μm.

remote ratio, 2.13±0.37, p=0.03) after MI. Tracer uptake also increased in the remote area (1.3-fold, p<0.04) at 4 weeks after MI compared to myocardium of sham-operated controls (Table 1).

PET Modeling

The distribution volume (DV) of [^{68}Ga]DOTA-E-[c(RGDfK)]$_2$ extracted from dynamic PET data by Logan graphical analysis was different between study groups and myocardial areas (Table 2). The average DV was higher in the infarct areas than either remote myocardium of MI rats or sham-operated rats. Logan plot-based DV correlated well both to the size of MI (r_s=0.753, p=0.019) and to other measures of [^{68}Ga]DOTA-E-[c(RGDfK)]$_2$ uptake—in vivo SUV at 45−60 min post-injection (r_s=0.747, p<0.001), ex vivo biodistribution (r_s=0.893, p=0.003), and autoradiography (r_s=0.562, p=0.01). Visual appearance of parametric Logan plot images and images generated with static SUV data appeared very similar (Fig. 3) as well.

The DV obtained with Logan graphical analysis using either metabolite-corrected or total plasma input function obtained from the LV cavity correlated closely (r_s=0.98, p< 0.001). The Logan plots also correlated with the binding potential (k1/k2) derived from compartmental analysis (r_s= 0.566, p=0.009). The binding potential (k1/k2) was higher in the MI than sham-operated rats, but plasma-to-tissue transport rate (k1) was comparable (Table 2). Only equilibrium volume of distribution (Vt) in the remote myocardium was different between MI and sham-operated animals (p= 0.04). More correlation results between variables are shown in Table 3.

Relationship Between Tracer Uptake and Histology

The increase in myocardial [^{68}Ga]DOTA-E-[c(RGDfK)]$_2$ uptake in the remote, non-infarcted myocardium coincided with the increase in interstitial collagen in this area by 4 weeks after MI (Figs. 1 and 2). However, there was no positive correlation between the amount of [^{68}Ga]DOTA-E-[c(RGDfK)]$_2$ uptake and collagen in the remote areas and actually an inverse correlation in the infarcted area (Fig. 4a, b). In the infarcted area, tracer uptake correlated closely (r_s= 1.000, p<0.001) to the area stained with integrin β_3 chain (CD61) (pooled 7 days and 4 weeks) antibodies (Fig. 4c) and the area stained with CD31 antibodies at 4 weeks (r_s= 0.83, p=0.021) (Fig. 4d), whereas there was no correlation (r_s=−0.25, p=0.26) to area of macrophage staining (pooled 7 days and 4 weeks) (Fig. 4e). In contrast to the infarcted area, the amount of positive immunostainings (CD31, CD61, and CD68) was low and could not be reliably quantified in the remote area.

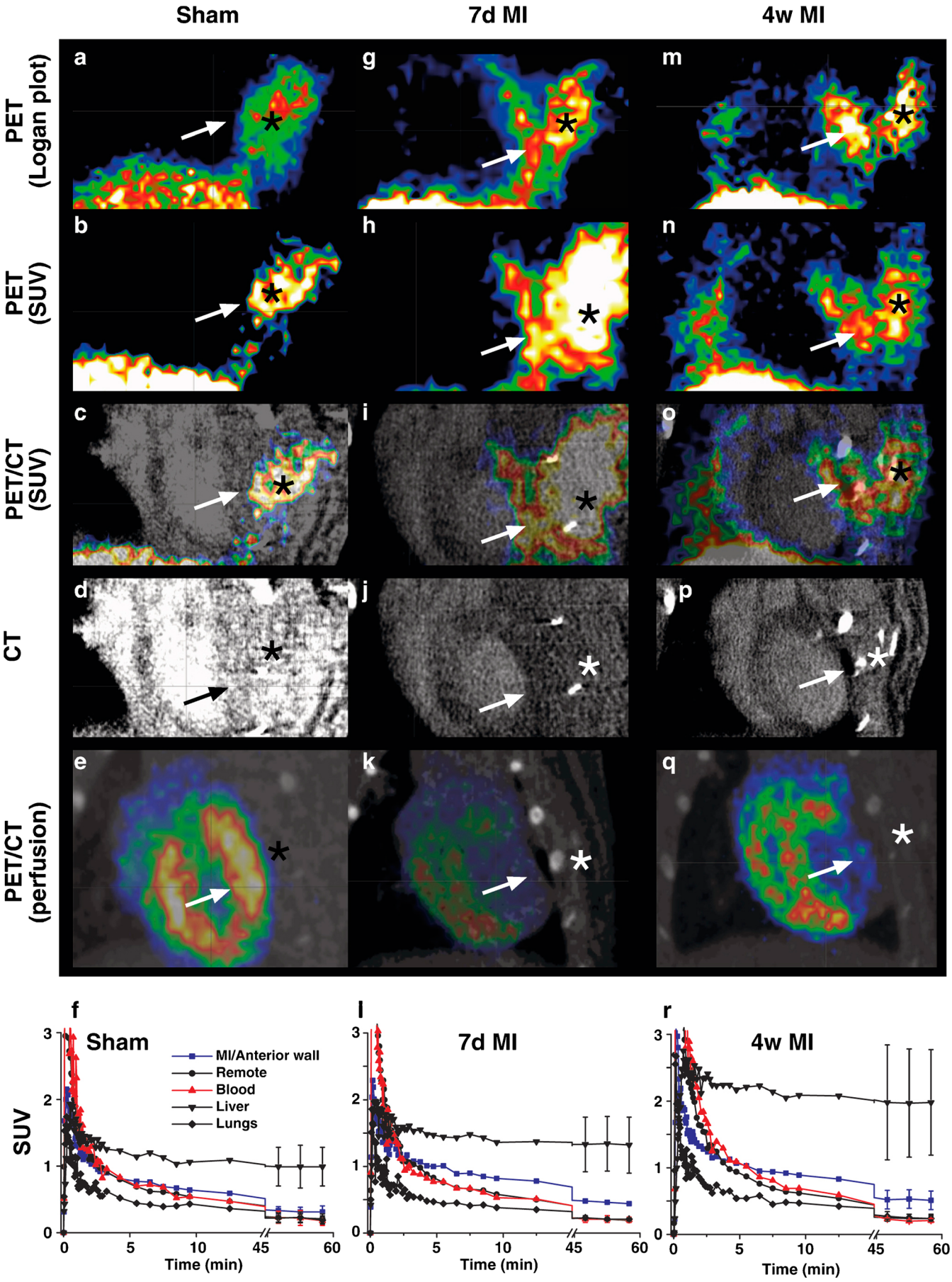
Sham
7d MI
4w MI
PET (Logan plot)
PET (SUV)
PET/CT (SUV)
CT
PET/CT (perfusion)
a
b
c
d
e
f
g
h
i
j
k
l
m
n
o
p
q
r
Sham
7d MI
4w MI
MI/Anterior wall
Remote
Blood
Liver
Lungs
SUV
Time (min)
0
5
10
45
60
1
2
3

◀ **Fig. 3.** In vivo imaging of rat myocardium. [68Ga]DOTA-E-[c(RGDfK)]$_2$ PET images expressed as Logan plot distribution volumes (DV) (a, g, m) and $SUV_{40–60\ min}$ (b, h, n), contrast-enhanced CT (d, j, p) and fused PET/CT images (c, i, p) demonstrate tracer uptake co-localizing with the anterior myocardial wall of the left ventricle (arrows) in coronal view of the chest at 7 days (middle column g–j) and 4 weeks (right column m–p) after MI, whereas uptake is low in a sham-operated rat (left column a–d). Extracardiac uptake is present in the thoracotomy scar (asterisk) in the chest wall. e, k, and q Myocardial perfusion imaging with [11C]acetate. There is perfusion defect consistent with anterior myocardial infarction in k and q, but perfusion is normal in e. Time-activity curves of average [68Ga]DOTA-E-[c(RGDfK)]$_2$ uptake are shown under the PET/CT images after sham operation (f), 7 days (l) and 4 weeks (r) after MI. Uptake in the liver (black triangles), lung (black diamonds), infarcted myocardium (blue box), remote myocardium in the septum (black circles), and blood (red triangles) are shown.

Table 2. Graphical and kinetic analysis of [68Ga]DOTA-E-[c(RGDfK)]$_2$ uptake

Study group, region	DV	Vt	K1	K1/k2
Pooled MI, infarction	1.01±0.23	1.36±0.27	0.16±0.05	0.55±0.14
Pooled MI, remote	0.64±0.07	0.98±0.37	–	–
Pooled sham, anterior wall	0.74±0.10	0.89±0.30	0.52±0.43	0.34±0.14
Pooled sham, remote	0.59±0.02	0.61±0.10	–	–
p values				
MI infarction vs. remote	0.001	0.05	–	–
MI infarction vs. sham anterior wall	0.01	0.04	0.19	0.046
MI remote vs. sham remote)	0.11	0.04	–	–

Results are expressed as mean ± SD and probability value (p) from Student's t test
DV distribution volume, Vt equilibrium volume of distribution, K1 plasma to tissue transport rate compartment model value, k2 tissue to plasma transport rate value, K1/k2 binding potential

Discussion

We found that [68Ga]DOTA-E-[c(RGDfK)]$_2$ peptide is potential tracer for in vivo monitoring of increased myocardial integrin expression associated with ECM remodeling after MI. Increased uptake of [68Ga]DOTA-E-[c(RGDfK)]$_2$ peptide in the rat myocardium after permanent coronary occlusion was confirmed by the ex vivo analyses. The uptake was highest in the infarcted area both at 7 days and 4 weeks after MI where it correlated with β_3 integrin expression. Interestingly, we also found increased tracer uptake in the remote, non-infarcted myocardium where it coincided with an increase in interstitial fibrosis by 4 weeks post-MI.

This is the first study to evaluate dimeric 68Ga-labeled RGD peptide for myocardial imaging. 68Ga tracers have the advantage of easy and fast radiolabeling with a generator-produced radionuclide. Our results confirm the findings of previous experimental studies using radiolabeled RGD peptides showing that $\alpha_v\beta_3$ integrin is strongly expressed in the myocardium for weeks after an ischemic injury [1–5, 10–12]. The results are also in line with a recent study evaluating uptake of monomeric and trimeric 68Ga-labeled cyclic RGD peptides in the infarcted rat myocardium [12]. From dimeric and tetrameric RGD peptides, the dimeric was considered as the best compromise between high uptake in the target and low uptake in nontarget organs like the kidney, liver, and intestines that could compromise cardiac imaging and cause radiation issues [6, 7]. A limitation of our study is that we were not able to do direct comparisons with other RGD-based tracers. In previous studies, RGD uptake in the infarcted area has been 3.9- to 5.2-fold higher than in the remote non-infarcted myocardium of MI rats as assessed by autoradiography [4, 5, 10–12]. Thus, the 5.1-fold (range, 3.7–8.3) higher uptake of [68Ga]DOTA-E-[c(RGDfK)]$_2$ is comparably high. The higher uptake ratio between infarcted area and myocardium of sham-operated rats (6.5 at 7 days) than the remote non-infarcted myocardium of MI rats in our study is explained by the increased tracer uptake also in the remote areas of MI rats. Comparison of in vivo imaging results between tracers is difficult in our model due to the limited spatial resolution of PET scanner, partial volume effects, spill over, and high positron energy of 68Ga. Therefore, autoradiography was considered as the preferable method for comparing the results between studies.

We found that it was feasible to detect increased integrin expression in the rat heart after MI in vivo using [68Ga]DOTA-E-[c(RGDfK)]$_2$ PET. Consistent with ex vivo analyses, in vivo imaging showed increased uptake both in the infarcted area and remote myocardium. Our study confirmed feasible kinetics.

Table 1. [68Ga]DOTA-E-[c(RGDfK)]$_2$ uptake in rat myocardium by in vivo PET imaging

	7 Days MI	4 Weeks MI	Pooled sham	p (7 days MI vs. sham)	p (4 weeks MI vs. sham)
MI	0.46±0.02	0.52±0.14	0.29±0.03	0.02	0.01
Remote	0.21±0.03	0.24±0.03	0.19±0.02	0.40	0.04
MI-to-remote	2.25±0.24	2.13±0.37	–	<0.001*	0.03*
Blood	0.20±0.06	0.21±0.02	0.17±0.04	0.27	0.21

Results are shown as average standardized uptake values (SUVs, mean ± SD) determined at 45−60 min after injection and probability value (p) from Student's t test
MI myocardial infarction
*p values MI vs. remote

Table 3. Correlations between variables when all groups and myocardial areas are pooled

	SUV (45−60 min)	DV	Vt
ARG (PSL/mm^2)[a]	0.677, 0.001	0.562, 0.010	0.431, 0.058
SUV (45–60 min)[a]		0.747, <0.001	0.652, 0.001
DV[a]	0.747, <0.001		0.816, <0.001
K1/k2[a]	0.541, 0.009	0.566, 0.006	0.718, <0.001
Infarct size (circ-%)[b]	0.000, 1.000	0.753, 0.010	0.714, 0.047
Collagen area (%)[b]	0.900, 0.019	−0.543, 0.133	−0.900, 0.037
ARG (PSL/mm^2)[b]	0.964, <0.001	0.893, 0.003	−0.071, 0.440
DV[b]	0.443, 0.136		0.750, 0.026
K1/k2[b]	0.429, 0.145	0.731, 0.040	0.643, 0.06

Results are expressed as r_s, p. (r_s Spearman's correlation coefficient, p probability value from Student's t test)
SUV standardized uptake value from in vivo PET determined at 45−60 min after injection, DV distribution volume, Vt equilibrium volume of distribution, ARG autoradiography, PSL/mm^2 photostimulated luminescense per square millimeter, K1/k2 binding potential from two-compartmental modeling, circ-% percentage of LV circumference
[a]All groups and myocardial areas pooled
[b]Infarct area

The tracer remained very stable (94±3.2 %) up to 45 min post-injection and metabolite correction of the PET data (up to 60 min post-injection) had only sparse effect on the results suggesting that they could be omitted and in so doing simplify modeling. Imaging results showed that SUV measurements in static images provided comparable results to kinetic modeling of distribution volume of tracer uptake simplifying in vivo analyses. Extracellular space augmentation in fibrotic areas could have influenced on high DV in the infarcted area, but that is most probably insignificant with long dynamic imaging and comparable SUV values. Furthermore, the fact that there was no difference in K1 values between infarcted and sham groups, indicate that tracer accumulation was independent of perfusion.

Uptake of [^{68}Ga]DOTA-E-[c(RGDfK)]$_2$ in the infarcted area correlated strongly with β_3 integrin expression, but not with the amount of macrophages that is consistent with previous studies [1–5, 12, 19]. The areal percentage of CD61 [β_3 integrin subunit] expression in the infarcted area was relatively low as compared with CD31, and CD61 expression was not confined to vascular structures by immunohistochemistry. This is in line with integrins involved in many parallel processes and expressed by many cell types during infarct healing and myocardial remodeling [23–25]. While β_3 integrin subunit has been mainly detected on endothelial and smooth muscle cells [23], it is possible that activated fibroblasts expressing $\alpha_v\beta_3$ and $\alpha_v\beta_5$ integrins are also in part responsible for RGD binding as has been previously shown by electron microscopy [4]. Surprisingly, however, an inverse correlation between the area of positive collagen staining and [^{68}Ga]DOTA-E-[c(RGDfK)]$_2$ uptake post-MI was found in the infarcted area that most probably indicates lowering of $\alpha_v\beta_3$ integrin expression in the final stages of the scar formation [3, 4]. Even though neovessel formation peaks at 1 week after the injury [1], a direct correlation between the area of positive CD31 staining and

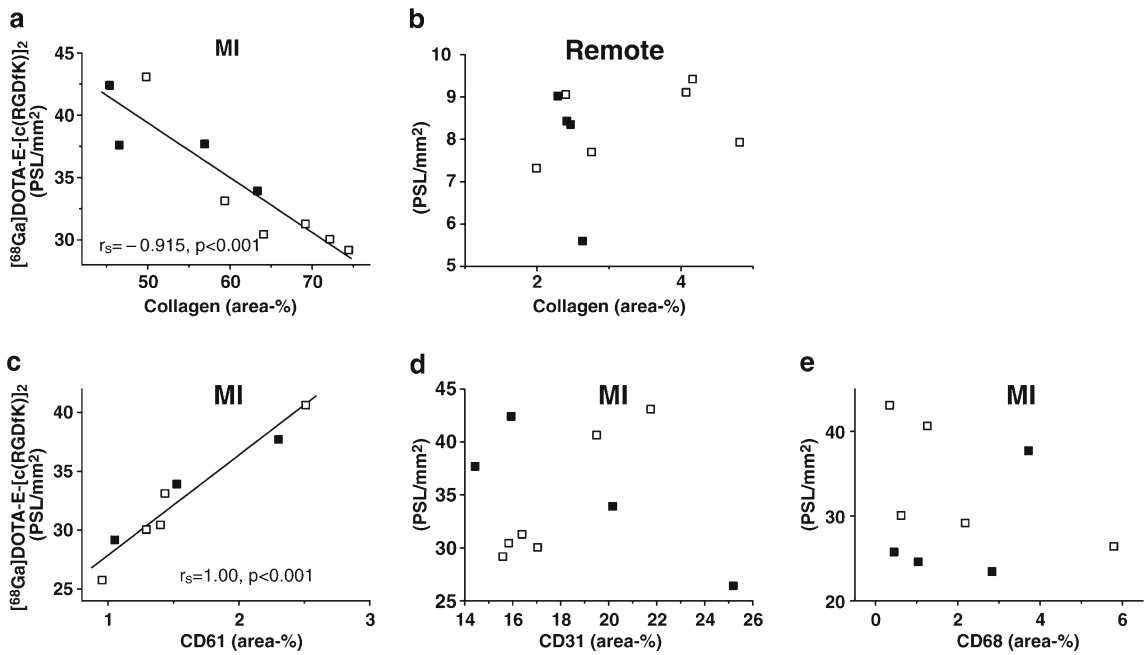

Fig. 4. Uptake of [^{68}Ga]DOTA-E-[c(RGDfK)]$_2$ versus histology. a, b Correlations between the amount of collagen (measured by Masson's trichrome staining) and uptake of [^{68}Ga]DOTA-E-[c(RGDfK)]$_2$ in rats with myocardial infarction. a Infarcted area, b remote area of myocardium. Accumulation of [^{68}Ga]DOTA-E-[c(RGDfK)]$_2$ in the infarcted area alone is compared with β_3 chain-positive staining (CD61, c), positive staining of capillaries (CD31, d), and macrophages (CD68, e). Correlations are expressed as r_s=Spearman's rank correlation coefficient. Filled boxes 7 days, hollow boxes 4 weeks. Statistical analysis showed very strong correlation between tracer uptake and the amount of β_3 chain, whereas correlation to neovessels could only be seen at 4 week time-point (r_s=0.83, p=0.021) (d). No correlation (r_s=–0.25, p=0.26) to macrophage staining could be observed.

[^{68}Ga]DOTA-E-[c(RGDfK)]$_2$ was visible at 4 weeks post-MI indicating a dominating role of angiogenesis as an RGD target in later stages of scar formation.

We found that in addition to the infarcted area, [^{68}Ga]DOTA-E-[c(RGDfK)]$_2$ uptake was also increased in the remote non-infarcted myocardium from 7 days after MI to 4 weeks by both ex vivo and in vivo analyses. Previously, van den Borne et al. found elevated uptake of RGD-based [^{99m}Tc]-CRIP at 12 weeks after MI in the remote myocardium in mice [4, 26], whereas some other studies have not reported such an increase [2, 5, 10, 11]. Multimerization has been shown to improve affinity of the RGD peptides that may be important for detecting changes in integrin expression in tissues with relatively low baseline expression levels, such as the myocardium. In the present study, increased [^{68}Ga]DOTA-E-[c(RGDfK)]$_2$ uptake coincided with the increase in interstitial fibrosis in the remote myocardium by 4 weeks post-MI despite the lack of direct correlation with the amount of interstitial collagen. The lack of correlation with the amount of mature, dense collagen does not exclude the possibility that this tracer reflects the formation myocardial fibrosis by detecting pathophysiological processes that precede the collagen deposition. Unfortunately, the small number of animals and limited amount of tissue precluded comprehensive analysis of the cellular mechanisms of [^{68}Ga]DOTA-E-[c(RGDfK)]$_2$ uptake in the remote myocardium. Detection of ECM alterations leading to formation of interstitial fibrosis outside the scar area could have important implications for detection of diffuse myocardial pathologies in the ischemic and non-ischemic myocardial diseases [25].

Conclusion

In conclusion, [^{68}Ga]DOTA-E-[c(RGDfK)]$_2$ peptide is a potential new tracer for PET imaging of increased integrin expression associated with ECM alterations in the infarcted and remote areas following MI.

Acknowledgments. The authors thank Erica Nyman and Liisa Lempiäinen for performing tissue sectioning and immunohistochemistry, Ville Aalto, M.Sc., with the CoE in Molecular Imaging, for the advice on the statistical analysis; Juho Virtanen, M.Sc., with the Turku PET Centre, for Image-J automatic analysis scripts; and Robert M. Badeau, Ph.D., with the University of Turku Language Center, for English language proofreading. The studies were conducted within the Finnish Centre of Excellence in Cardiovascular and Metabolic Diseases supported by the Academy of Finland, the University of Turku, the Turku University Hospital, and the Åbo Akademi University. This study was financially supported by the Turku University Hospital, Sigrid Juselius Foundation, Finnish Cultural Foundation, and Finnish Foundation for Cardiovascular Research.

Conflict of Interest. The authors declare that they have no conflict of interest.

References

1. Meoli DF, Sadeghi MM, Krassilnikova S et al (2004) Noninvasive imaging of myocardial angiogenesis following experimental myocardial infarction. J Clin Invest 113:1684–1691
2. Higuchi T, Bengel FM, Seidl S et al (2008) Assessment of alphavbeta3 integrin expression after myocardial infarction by positron emission tomography. Cardiovasc Res 78:395–403
3. van den Borne SW, Diez J et al (2010) Myocardial remodeling after infarction: the role of myofibroblasts. Nat Rev Cardiol 7:30–37
4. van den Borne SW, Isobe S, Verjans JW et al (2008) Molecular imaging of interstitial alterations in remodeling myocardium after myocardial infarction. J Am Coll Cardiol 52:2017–2028
5. Sherif HM, Saraste A, Nekolla SG et al (2012) Molecular imaging of early alphavbeta3 integrin expression predicts long-term left-ventricle remodeling after myocardial infarction in rats. J Nucl Med 53:318–323
6. Dijkgraaf I, Kruijtzer JA, Liu S et al (2007) Improved targeting of the alphavbeta3 integrin by multimerisation of RGD peptides. Eur J Nucl Med Mol Imaging 34:267–273
7. Dijkgraaf I, Yim CB, Franssen GM et al (2011) PET imaging of alphavbeta3 integrin expression in tumours with 68Ga-labelled mono-, di- and tetrameric RGD peptides. Eur J Nucl Med Mol Imaging 38:128–137
8. Dijkgraaf I, Terry SY, McBride WJ et al (2013) Imaging integrin alpha-v-beta-3 expression in tumors with an 18 F-labeled dimeric RGD peptide. Contrast Media Mol Imaging 8:238–245
9. Hua J, Dobrucki LW, Sadeghim MM et al (2005) Noninvasive imaging of angiogenesis with a 99mTc-labeled peptide targeted at alphavbeta3 integrin after murine hindlimb ischemia. Circulation 111:3255–3260
10. Gao H, Lang L, Guo N et al (2012) PET imaging of angiogenesis after myocardial infarction/reperfusion using a one-step labeled integrin-targeted tracer 18 F-AlF-NOTA-PRGD2. Eur J Nucl Med Mol Imaging 39:683–692
11. Menichetti L, Kusmic C, Panetta D et al (2013) MicroPET/CT imaging of αvβ3 integrin via a novel 68Ga-NOTA-RGD peptidomimetic conjugate in rat myocardial infarction. Eur J Nucl Med Mol Imaging 40:1265–1274
12. Laitinen I, Notni J, Pohle K et al (2013) Comparison of cyclic RGD peptides for αvβ3 integrin detection in a rat model of myocardial infarction. EJNMMI Res 3:38
13. Pfeffer MA, Pfeffer JM, Fishbein MC et al (1979) Myocardial infarct size and ventricular function in rats. Circ Res 44:503–512
14. Sherif HM, Saraste A, Weidl E et al (2009) Evaluation of a novel 18 F-labeled positron-emission tomography perfusion tracer for the assessment of myocardial infarct size in rats. Circ Cardiovasc Imaging 2:77–84
15. Dijkgraaf I, Rijnders AY, Soede A et al (2007) Synthesis of DOTA-conjugated multivalent cyclic-RGD peptide dendrimers via 1,3-dipolar cycloaddition and their biological evaluation: implications for tumor targeting and tumor imaging purposes. Org Biomol Chem 5:935–944
16. Dijkgraaf I, Kruijtzer JA, Frielink C et al (2006) Synthesis and biological evaluation of potent alphavbeta3-integrin receptor antagonists. Nucl Med Biol 33:953–961
17. Seppälä J, Seppänen M, Arponen E, Lindholm P, Minn H (2009) Carbon-11 acetate PET/CT based dose escalated IMRT in prostate cancer. Radiother Oncol 93:234–240
18. Haukkala J, Laitinen I, Luoto P et al (2009) 68Ga-DOTA-RGD peptide: biodistribution and binding into atherosclerotic plaques in mice. Eur J Nucl Med Mol Imaging 36:2058–2067
19. Laitinen I, Saraste A, Weidl E et al (2009) Evaluation of alphavbeta3 integrin-targeted positron emission tomography tracer 18 F-galacto-RGD for imaging of vascular inflammation in atherosclerotic mice. Circ Cardiovasc Imaging 2:331–338
20. Silvola JM, Saraste A, Forsback S et al (2011) Detection of hypoxia by [18 F]EF5 in atherosclerotic plaques in mice. Arterioscler Thromb Vasc Biol 31:1011–1015
21. Zhang X, Xiong Z, Wu Y et al (2006) Quantitative PET imaging of tumor integrin alphavbeta3 expression with 18 F-FRGD2. J Nucl Med 47:113–121
22. Kim JH, Kim YH, Kim YJ et al (2013) Quantitative positron emission tomography imaging of angiogenesis in rats with forelimb ischemia using 68Ga-NOTA-c(RGDyK. Angiogenesis 16:837–846
23. Manso AM, Kang SM, Ross RS (2009) Integrins, focal adhesions, and cardiac fibroblasts. J Investig Med 57:856–860
24. Kuppuswamy D, Kerr C, Narishige T et al (1997) Association of tyrosine-phosphorylated c-Src with the cytoskeleton of hypertrophying myocardium. J Biol Chem 272:4500–4508
25. Higuchi T, Wester HJ, Schwaiger M (2007) Imaging of angiogenesis in cardiology. Eur J Nucl Med Mol Imaging 34:S9–S19
26. van den Borne SW, Isobe S, Zandbergen HR et al (2009) Molecular imaging for efficacy of pharmacologic intervention in myocardial remodeling. J Am Coll Cardiol 2:187–198